Journal of Chromatography A, 1218 (2011) 5487–5497

Contents lists available at ScienceDirect

Journal of Chromatography A

journal homepage: www.elsevier.com/locate/chroma

An improved capillary model for describing the microstructure characteristics, fluid hydrodynamics and breakthrough performance of proteins in cryogel beds

Junxian Yun[a,b,*], Gry Ravn Jespersen[a,c], Harald Kirsebom[a], Per-Erik Gustavsson[c], Bo Mattiasson[a], Igor Yu Galaev[a,d,1]

[a] Department of Biotechnology, Lund University, P.O. Box 124, SE-22100 Lund, Sweden
[b] State Key Laboratory Breeding Base of Green Chemistry Synthesis Technology, College of Chemical Engineering and Materials Science, Zhejiang University of Technology, Chaowang Road 18, Hangzhou 310032, Zhejiang Province, China
[c] Department of Biopharm Chemistry, Novo Nordisk A/S, DK-2760 Måloev, Denmark
[d] DSM Food Specialties B.V., P.O. Box 1, 2600 MA Delft, The Netherlands

ARTICLE INFO

Article history:
Received 31 January 2011
Received in revised form 19 May 2011
Accepted 9 June 2011
Available online 22 June 2011

Keywords:
Cryogel
Mathematical model
Pore size distribution
Tortuosity
Skeleton thickness
Protein

ABSTRACT

A capillary-based model modified for characterization of monolithic cryogels is presented with key parameters like the pore size distribution, the tortuosity and the skeleton thickness employed for describing the porous structure characteristics of a cryogel matrix. Laminar flow, liquid dispersion and mass transfer in each capillary are considered and the model is solved numerically by the finite difference method. As examples, two poly(hydroxyethyl methacrylate) (pHEMA) based cryogel beds have been prepared by radical cryo-copolymerization of monomers and used to test the model. The axial dispersion behaviors, the pressure drop vs. flow rate performance as well as the non-adsorption breakthrough curves of different proteins, i.e., lysozyme, bovine serum albumin (BSA) and concanavalin A (Con A), at various flow velocities in the cryogel beds are measured experimentally. The lumped parameters in the model are determined by matching the model prediction with the experimental data. The results showed that for a given cryogel column, by using the model based on the physical properties of the cryogel (i.e., diameter, length, porosity, and permeability) together with the protein breakthrough curves one can obtain a reasonable estimate and detailed characterization of the porous structure properties of cryogel matrix, particularly regarding the number of capillaries, the capillary tortuousness, the pore size distribution and the skeleton thickness. The model is also effective with regards to predicting the flow performance and the non-adsorption breakthrough profiles of proteins at different flow velocities. It is thus expected to be applicable for characterizing the properties of cryogels and predicting the chromatographic performance under a given set of operating conditions.

1. Introduction

Monolithic cryogels have recently been proposed as a new class of chromatographic supports for separation of biomolecules in downstream processes [1–3]. Numerous studies have been carried out on the preparation of cryogels [4–14], graft polymerization and modification of the cryogel matrix [15–21], characterization of the cryogel properties and adsorption behaviors [6,7,22–25], as well as cryogel applications in capturing various target biomolecules, cells and viruses from crude feedstocks or suspensions [5,26–35]. Cryogel beds could be prepared with a wide variety of different pore size distributions, microstructures, binding capacities, permeabilities and behaviors of hydrodynamic dispersion, breakthrough and elution. The essential part of the preparation of cryogels is freezing of the reaction mixture, which is a stochastic process. Hence each cryogel sample is somewhat unique and has its own physical properties, and thus, specific hydrodynamic and chromatographic behavior towards a given target feedstock. Non-destructive methods for characterization of the sample porosity are of crucial importance for a development of reproducibly performing commercial product. Modeling of fluid flow and mass transfer within cryogel beds as well as characterization of the matrix are of great relevance and fundamental to unraveling of the properties of cryogels. Such insights will promote development of new cryogels and thus expand the applications of the monolithic format in chromatographic separations. Due to the complexity of the pore network system within cryogels, it is still a challenging task to develop a detailed model for characterizing the porous properties of a cryogel

* Corresponding author at: College of Chemical Engineering and Materials Science, Zhejiang University of Technology, Chaowang Road 18, Hangzhou 310032, China Tel.: +86 571 88320951; fax: +86 571 88033331.
E-mail addresses: yunjx@zjut.edu.cn (J.X. Yun), Igor.galaev@dsm.com (I.Y. Galaev).
[1] Present address: DSM Food Specialties B.V., P.O. Box 1, 2600 MA Delft, Alexander Fleminglaan 1, 2613 AX Delft, The Netherlands. Tel.: +31 15 2793771; fax: +31 15 2794110.

0021-9673/$ – see front matter © 2011 Elsevier B.V. All rights reserved.
doi:10.1016/j.chroma.2011.06.056

matrix and describing the chromatographic adsorption and breakthrough behaviors of macromolecules such as proteins.

Numerous mathematical models have been developed to describe the fluid flow and mass transfer characteristics in fixed beds and monoliths in the past years, for instance [36–49]. Some well-validated models in packed beds, such as the equilibrium-dispersive model, the lumped pore diffusion model and the classical random-walk model of Giddings [50], were also employed to investigate the adsorption–desorption and mass transfer kinetics and breakthrough profiles in monolith columns [51,52]. However, the chromatographic and transport characteristics between the monoliths and packed beds are very different due to their different microstructures and these models are needed to be modified. Actually, the fluid hydrodynamics and mass transfer behaviors in monolith beds depend strongly on the micro-structural properties of pores and skeletons. Several approaches have been proposed by considering the detailed structural properties of monoliths in literatures [37,38,50–70], also as reviewed recently in Refs. [71–73]. The Kozeny–Carman approach derived from packed beds has been suggested to calculate the hydraulic permeability and the dispersion behaviors in monolith columns [53–58]. In this approach the porous structure of a monolith was assumed to be made up of uniform spheres together with the interstitial void spaces between these spheres. Unfortunately, incorrect results could be obtained by direct using the Kozeny–Carman equation to characterize monolith beds. For monolith beds, parameters such as the equivalent sphere diameter, the domain size or the equivalent dispersion particle diameter, were proposed alternatively to replace the particle diameter in Kozeny–Carman equation. Due to the complicated and tortuous morphology of pores and skeletons existing in monoliths, this method found its applications limited mainly in silica monolith rods. Meyers and Liapis [37] developed an approach by employing a pore network model to investigate the liquid flow, solute diffusion and breakthrough dynamic behaviors in monoliths. In their model the porous structure of interconnected pores was represented by a regular cubic lattice including pore bonds and nodes [38]. As one knows that huge numbers of pores exist in an actual monolithic column and it is in some cases difficult to construct a network close to a real monolith. Furthermore, the pore structures and shapes of monoliths are so complicated that it is still a challenge to accurately determine the key parameters such as pore connectivity in network models. Miyabe and Guiochon [59] suggested a model by considering the monolith as continuous porous unit structure consisting of cylindrical skeletons surrounded by through-macropores. The bed was assumed homogeneous and thus the general kinetic model could be solved to analyze peak broadening, dispersion and mass transfer kinetics [60,61]. By combining the homogeneous cylindrical unit model and the network model, Gritti et al. [62] developed the parallel pore and pore network models to predict exclusion curves for inverse size-exclusion chromatography. In recent years, the morphology reconstruction approach combining Computational Fluid Dynamics (CFD) and imaging techniques have also been introduced in monolith modeling by several groups [63–69]. The so-called tetrahedral skeleton model was proposed to reconstruct more complicated geometrical structure close to the internal structures of monoliths. This interest model has been demonstrated to be useful and effective in the simulation of the mobile phase transport and hydrodynamics in silica monoliths. However, numerical calculation of concentration fields in such a complicated model for an actual monolith is a challenging task. Recently, Trilisky et al. [70] developed a model by constructing the monolith based on the 2D electron images of pore geometry. The protein breakthrough curves and binding capacities were calculated by considering the pore size distributions.

Common to these monoliths or particulate adsorbents is, that they all have pore diameters which are close to or below micron scale, and thus, primarily diffusional transport occurs within these small pores, although in some macropores of monoliths or interstitial voids of particulate packed beds convective transport also exists during the procedure of chromatography. Polymer-based or silica-based monoliths even have porous structures with both small mesopores and large through-pores, and consequently complex transport behaviors within these wide-scale bimodal pores [56,71–73]. However, the sizes of pores in cryogels are in the range from a few to hundreds of microns [1–5,9,26], which is much larger than that within the conventional monolithic beds. Due to the cryo-polymerization under frozen conditions during the formation of cryogels, the monomers were concentrated by the formation of ice crystals. The polymerization was then achieved at high local-concentration conditions and very dense and thin skeleton was produced. In this skeleton of high polymer concentration very few mesopores exists or very few of them are available for chromatography at low column pressures (much lower than those in conventional monoliths like silica monoliths). Therefore, the microstructures of pores and skeleton within cryogels are much different as those in conventional monoliths having multi-scale pores. In cryogel beds, supermacropores are predominate and the contributions of small skeleton mesopores to the liquid flow and transport of macromolecules like proteins are very limited and thus could be neglected. Within those supermacropores, convective laminar flow is expected to be the dominating means of transport.

Capillary model is a simplification approach of porous media with macropores like the packed beds of perfusive adsorbents and the macroporous silica monoliths, in which the bed was assumed to consist of a bundle of capillaries [41,42,44,45,50,74]. Zabka et al. [41,42] developed a capillary model for silica-based monoliths by assuming the bed as equal parallel capillaries with silica skeletons. In their model, both the diffusion mass transfer within the skeleton and the laminar flow, the parabolic velocity profile, as well as the axial and radial diffusion in capillaries were considered. Actually, the morphology of supermacropores in cryogels is close to the distorted cannular shape and the skeletons are very thin, thereby making the capillary model a simple and easy but interest and effective representation approach for actual cryogels. Persson et al. have proposed a capillary-based model for the characterization of properties and the description of mass transfer and chromatographic adsorption within cryogel beds [22]. In the model, the cryogel was assumed to be made up of several groups of capillaries. These capillaries had equal length as that of the cryogel itself and the skeleton thickness was neglected. The model was demonstrated to be effective in describing protein adsorption performance in a 10 mm diameter cryogel column. Based on this work, we have recently developed a model for the description of protein adsorption and mass transfer behaviors by considering the overall axial dispersion [75].

In this work, we present an improved model by considering the actual detailed properties of the cryogel microstructure, e.g., the tortuosities of pores and the skeleton thickness and consequently a numerical method for solving the differential equations in the model is proposed. Experimental data of proteins from two pHEMA cryogel beds under non-adsorption conditions are matched and compared to the model prediction. The corresponding lumped parameters in the model are determined and the overall results and applicability of the model are discussed.

2. Model

A cryogel is made up of dense polymer skeletons with varying thickness and many pores of different sizes. The skeletons provide the mechanical support and the sites of functional groups for the adsorption of target biomolecules, while the pores permit the flow

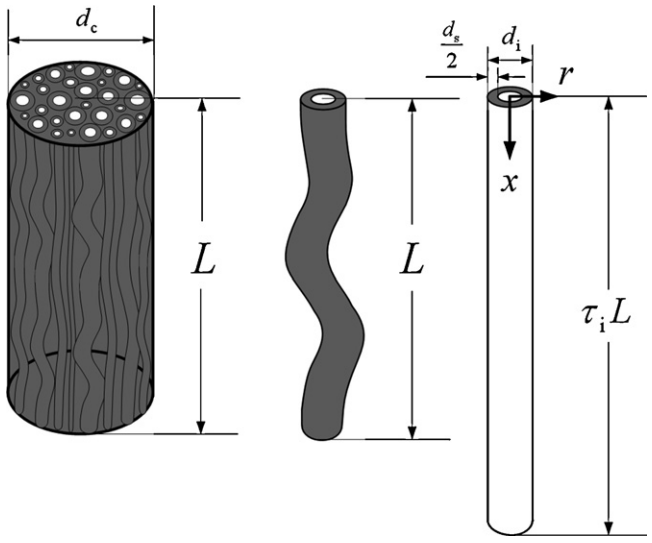

Fig. 1. The schematic diagram of a cryogel made up of tortuous capillaries.

of liquids through the gel. These pores are interconnected and form a complicated network system for the liquid fluid flow and mass transfer of target molecules.

In the present model, the cryogel is assumed to be made up of capillaries with a given size distribution, similar to those in references [22,41,42,44,50,74]. Here, however, we assumed these capillaries are not straight but tortuous. The interconnectivity among capillaries was ignored because the skeleton is thin and the pore sizes are large. The inlets of capillaries are all located at the cryogel inlet surface and their outlets are located at the cryogel outlet surface. They have different lengths and tortuosities. In order to simplify the model, the polymer skeleton outside each capillary is assumed to have a constant thickness, i.e., half of the skeleton thickness d_s.

2.1. Cryogel microstructure and porosity

Fig. 1 displays schematically a cryogel structure made up of capillaries with different length and tortuosities.

For a given capillary i, the tortuosity τ_i is defined as

$$\tau_i = \frac{L_i}{L} \tag{1}$$

where L_i is the capillary length and L the length of the cryogel, respectively.

The porosity of the cryogel bed φ is determined by the total volume of capillaries and the bed volume:

$$\varphi = \frac{\pi}{4A}\sum_{i=1}^{N_g} n_i d_i^2 \tau_i \tag{2}$$

where A ($= \pi d_c^2/4$, d_c is the cryogel diameter) is the cross-area of the cryogel bed, N_g the total number of capillary groups with the same diameter, d_i the capillary diameter and n_i the number of capillaries in group i, respectively. It is assumed that capillaries in a given group have the same diameter, length, tortuosity and skeleton thickness.

The total volume of capillaries and skeleton walls is equal to the bed volume, thus

$$\frac{\pi}{4A}\sum_{i=1}^{N_g} n_i (d_i + d_s)^2 \tau_i = 1 \tag{3}$$

2.2. Fluid flow within a capillary and permeability of the cryogel

In most practical cases, liquid flow in these capillaries is laminar due to the low Reynolds number. The flow rate in a capillary i can then be calculated by the Hagen-Poiseuille equation, as described in [22,74]:

$$Q_i = \frac{\pi d_i^4 \Delta p_i}{128 \mu_L L_i} \tag{4a}$$

where μ_L is the liquid viscosity, Q_i the flow rate and Δp_i the pressure drop between the inlet and outlet of the capillary i, respectively.

The pressure drop of each capillary is equal to that of the whole cryogel Δp. Then, Eq. (4a) is re-written as

$$Q_i = \frac{\pi d_i^4 \Delta p}{128 \mu_L \tau_i L} \tag{4b}$$

The total flow rate in the cryogel bed Q is given by

$$Q = \frac{\pi \Delta p}{128 \mu_L L}\sum_{i=1}^{N_g} \frac{n_i d_i^4}{\tau_i} \tag{5}$$

At a given pressure drop, the flow rate in the cryogel bed can also be calculated by Darcy's equation

$$Q = \frac{kA\Delta p}{\mu_L L} \tag{6}$$

where k is the fluid permeability of the cryogel bed.

Combining Eqs. (5) and (6) one can obtain

$$\frac{\pi}{128kA}\sum_{i=1}^{N_g} \frac{n_i d_i^4}{\tau_i} = 1 \tag{7}$$

A size distribution of capillary diameters with a probability density function $f_1(d_i)$ is assumed. Since the capillary diameters are in the range from the minimum pore diameter d_{min} to the maximum pore diameter d_{max} within cryogels, the actual probability density function for the capillary diameter distribution $f(d_i)$ can be expressed as (similarly as that in expanded beds by Yun et al. [76])

$$f(d_i) = \frac{f_1(d_i)}{1 - \int_{-\infty}^{d_{min}} f_1(d_i)\,\delta d_i - \int_{d_{max}}^{+\infty} f_1(d_i)\delta d_i} \tag{8a}$$

For a normal distribution, the probability density function for capillary diameters is given by

$$f(d_i) = \frac{(1/\sqrt{2\pi}\sigma)\exp[-(d_i - d_m)^2/2\sigma^2]}{1 - \int_{-\infty}^{d_{min}} (1/\sqrt{2\pi}\sigma)\exp[-((d_i - d_m)^2/2\sigma^2)]\delta d_i - \int_{d_{max}}^{+\infty} (1/\sqrt{2\pi}\sigma)\exp[-((d_i - d_m)^2/2\sigma^2)]\delta d_i} \tag{8b}$$

where σ is the standard deviation and d_m the mean diameter of capillaries in the cryogel column.

2.3. Mass transfer and dispersion in the mobile fluid phase

For a cryogel without ligands, biomolecules would pass through the pores freely and no adsorption would occur. Therefore, under

this non-adsorption condition the differential mass balance equation of biomolecules in the mobile fluid phase of the tortuose capillary i can be written as following by modifying the axial dispersed mass balance equation for plug flow [22,49,74]

$$\frac{\partial C_{Di}(x_D, t_{Di})}{\partial t_{Di}} = \frac{1}{Pe_i}\frac{\partial^2 C_{Di}(x_D, t_{Di})}{\partial x_D^2} - \frac{\partial C_{Di}(x_D, t_{Di})}{\partial x_D} \tag{9a}$$

The initial and the boundary conditions are expressed as

$$C_{Di}(x_D, t_{Di})\big|_{t_{Di}=0, x_D>0} = 0 \tag{9b}$$

$$C_{Di}(x_D, t_{Di})\big|_{x_D=0} = 1 \tag{9c}$$

$$\left.\frac{\partial C_{Di}(x_D, t_{Di})}{\partial x_D}\right|_{x_D=1} = 0 \tag{9d}$$

where $C_{Di}(x_D, t_{Di})$ ($=C_i(x,t)/C_0$, $C_i(x,t)$ is the bulk-phase concentration and C_0 the inlet concentration) is the dimensionless bulk-phase concentration of biomolecules in the capillary i, x_D ($=x/\tau_i L$, x is the distance) the dimensionless distance from the inlet along the capillary length, t_{Di} ($=tU_i/\tau_i L$, where the velocity $U_i = U_L d_i^2/32k\tau_i$, t is the time and $U_L = Q/A$ is the liquid flow velocity in the cryogel bed) the dimensionless time, Pe_i ($=\tau_i L U_i/D_{axi}$, D_{axi} is the axial liquid dispersion coefficient) the axial Peclet number, respectively.

For laminar flow in a straight tube, the axial dispersion coefficient can be estimated by Taylor–Aris correlation [77–81], which was based on the work originally by Taylor in 1950s [82]:

$$D_{axi} = D_{AB} + \frac{U_i^2 d_i^2}{192 D_{AB}} \tag{10a}$$

where D_{AB} is the molecular diffusion coefficient of biomolecules. In the present case, however, the capillary is tortuous. In comparison with the straight tube the axial dispersion in a tortuous tube is more complicated because the tortuosity could induce the local secondary flow and variation of residence time across the flow, as those observed in coiled tubes or helical channels [83,84]. Basically, the axial dispersion coefficient in a curved tube is influenced by several factors, such as the flow velocity profile, the fluid properties, the tube diameter and tortuosity, and even the alternating curvatures. All these factors could contribute to the longitudinal molecular diffusion and the radial mass transfer and thus, the changing of the axial dispersion coefficient in comparison with that for straight tubes. For laminar flow in the present tortuous capillary, there is a lack of precise correlations for the axial dispersion coefficient. Recently, Gutsche and Bunke [45] obtained a modified correlation of the axial dispersion coefficient in fixed beds. In their correlation, the contributions of the bed tortuosity and the bed skeleton (i.e., adsorbents) to the axial dispersion were included and the deviations from the ideal flow and mixing behavior were described by using a dimensionless parameter, which was determined according to the experimental measurements. Based on the correlation suggested by Gutsche and Bunke [45], we use the following correlation to estimate D_{axi} in the present tortuous capillary

$$D_{axi} = \frac{D_{AB}}{\tau_i} + \frac{1}{\psi}\frac{U_i^2 d_i^2}{192 D_{AB}} \tag{10b}$$

The parameter $\psi = \zeta Pe_{AB}^{0.775}$ in a fixed bed and the constant ζ depends on the adsorbents used ($\zeta = 0.011$ and 0.018 for regular and irregular adsorbents, respectively [45]). For a tortuous capillary in a cryogel bed, ζ should depend on the shape and thickness of the skeletons and thus can also be assumed to be a constant. The molecule Peclet number in capillary i can be expressed as $Pe_{ABi} = d_i U_i/D_{AB}$ and then $\psi = \zeta Pe_{ABi}^{0.775}$. In this model, the correlation by Gutsche and Bunke [45] is used for each capillary, i.e., $\psi = 0.018 Pe_{ABi}^{0.775}$.

2.4. Tortuosity of capillaries

In the above model, it is necessary to determine the unknown parameter τ_i. As can be seen from Eq. (4b), at a given pressure drop the time for fluid flow through a capillary with larger diameter and smaller tortuosity could be much shorter than that for a small one with larger tortuosity. In such case, the broad residence time distribution (RTDs) for fluid through could occur in a cryogel bed with the wide size distribution of capillaries, which implies that strong dispersion could always be observed. However, the axial dispersion in many real cryogels with pore diameters in the range from 10 to 200 μm is not strong but weak (the axial dispersion coefficient 10^{-6} to 10^{-8} m^2/s) and the RTD curves are not broad either [9–11,20,21,32]. This reveals that the larger capillaries might be longer or more tortuous than that of the smaller ones, which could result in the narrow RTDs and weak axial dispersion. Therefore, in this work we assume the following linear function for describing the variation of τ_i vs. the capillary diameter:

$$\tau_i = \tau_{d\,min} + \varpi(d_i - d_{min}) \tag{11a}$$

where τ_{dmin} (≥ 1) is the tortuosity of the capillary with diameter d_{min} and the parameter ϖ is the line slope of the tortuosity vs. capillary diameter.

Actually, the tortuosity τ_{dmax} of the capillary with diameter d_{max} can be determined from the RTDs or breakthrough curves using a non-adsorbent tracer. The time for the tracer passing through the largest capillary within the cryogel bed is expressed as

$$t_{d\,max} = \frac{\tau_{d\,max} L}{U_{d\,max}} = \frac{\tau_{d\,max} L}{U_L d_{max}^2} 32k\tau_{d\,max} \tag{11b}$$

where U_{dmax} is the liquid velocity within the capillary with the diameter d_{max}. Then, ϖ is determined and Eq. (11a) can be rewritten as

$$\tau_i = \tau_{d\ min} + \frac{(d_i - d_{min})}{(d_{max} - d_{min})}\left(\sqrt{\frac{t_{d\,max} U_L}{32kL}} d_{max} - \tau_{d\ min}\right) \tag{11c}$$

In most practical cases, however, it is difficult to determine τ_{dmin} directly from the RTDs or breakthrough curves due to the extended tails of these curves. The parameter can then be determined by fitting the permeability and porosity as well as the protein breakthrough data of the cryogel bed.

3. Numerical methods

For a given cryogel bed, the unknown parameters τ_{dmin}, d_s, σ, d_m and the total number of capillaries M ($= \sum_{i=1}^{N_g} n_i$) in the model were estimated by fitting Eqs. (2), (3), (7) and (9a) together with the experimental data and restricting d_s and M in certain limits.

For a typical class of cryogels prepared under similar conditions, the skeleton thickness varies in a relatively narrow range as observed in experiments [2–11,22], e.g., 4–24 μm for the polyacrylamide-based cryogels prepared by Persson et al. [22] and Yao et al. [20]. Therefore, in this model the value of d_s is restrained in a given range. The range of M was estimated by considering different situations. In the case that all the capillaries have the same diameter of d_{min}, the maximum number of capillaries M_{max} can be obtained by regarding the total volume of these capillaries as equal to the cryogel bed and from Eq. (4a)

$$\frac{M_{max}\pi(d_{min} + d_s)^2 \tau_{d\ min} L}{4} = \frac{\pi d_c^2 L}{4} \tag{12a}$$

In the case that all the capillaries have the same diameter of d_{max}, the minimum value M_{min} can also be achieved in a similar way and we get

$$\frac{M_{max}\pi(d_{min}+d_s)^2\tau_{d\ max}L}{4}=\frac{\pi d_c^2 L}{4} \tag{12b}$$

Then,

$$M_{max,1}=\frac{d_c^2}{(d_{min}+d_s)^2\tau_{d\ min}} \tag{12c}$$

$$M_{min,1}=\frac{d_c^2}{(d_{max}+d_s)^2\tau_{d\ max}} \tag{12d}$$

On the other hand, M_{max} or M_{min} are obtained by regarding the cross-section areas of these capillaries equal to the cross-area of the cryogel bed due to the fact that all the inlets of capillaries (along each of the capillary axis) should be distributed on the surface of the cryogel bed inlet.

$$M_{max,2}=\frac{d_c^2}{(d_{min}+d_s)^2} \tag{12e}$$

$$M_{min,2}=\frac{d_c^2}{(d_{max}+d_s)^2} \tag{12f}$$

Therefore, for an actual cryogel the possible value of M should be in the following range

$$\mathrm{Max}(M_{min,1}, M_{min,2}) \le M \le \mathrm{Min}(M_{max,1}, M_{max,2}) \tag{13a}$$

i.e.,

$$M_{min,2} \le M \le M_{max,1} \tag{13b}$$

Eq. (13b) was employed as one constrained condition and the possible value of M was then determined by matching the model calculation with the experimental data.

The finite difference method was then employed to solve the mass balance equation in the model, as that reported in [22]. The discrete procedure is also similar as that reported by Özdural et al. [40] and Yun et al. [76]. The mass balance equation was discretized by the central difference approximation for $\partial C_{Di}/\partial x_D$ and $\partial^2 C_{Di}/\partial x_D^2$ and the implicit scheme of finite difference with the backward difference approximation for $\partial C_{Di}/\partial t_{Di}$. The concentration at the out let of the cryogel bed was obtained by averaging the concentrations in capillaries based on their flow rates and written as

$$C=\frac{\sum_{i}^{N_g} C_i n_i Q_i}{Q} \tag{14}$$

The deviations of the model predictions from the experimental data of the porosity, permeability, the bed volume as well as the protein breakthrough were estimated by calculating the differences between the predicted (subscript symbol is "cal") and experimental data (subscript symbol is "exp"). The relative difference of the porosity is given by

$$\delta_\phi=\frac{|\varphi_{cal}-\varphi_{exp}|}{\varphi_{exp}} \tag{15a}$$

The relative difference of the permeability is expressed as

$$\delta_k=\frac{|k_{cal}-k_{exp}|}{k_{exp}} \tag{15b}$$

The relative difference of the bed volume is defined as

$$\delta_V=\frac{|V_{cal}-V_{exp}|}{V_{exp}} \tag{15c}$$

where V_{cal} and V_{exp} are the predicted and experimental volumes of the cryogel, respectively.

The mean dimensionless difference of the breakthrough data is expressed as

$$\delta_C=\frac{\sum_{j=1}^{N_j}|C_{cal,j}-C_{exp,j}|}{N_j C_0} \tag{15d}$$

where N_j is the total data number of the experimental breakthrough.

4. Experimental

4.1. Materials

Hydroxyethyl methacrylate (HEMA, 96%), was purchased from Acros Organics. Allyl glycidyl ether (AGE, 99%), poly(ethyleneglycol) diacrylate (PEGDA, 99%, $M_n \sim 258$ g/mol), iminodiacetic acid (IDA, 98%), *N*,*N*,*N*′,*N*′-tetramethylethylenediamine (TEMED, 99%), ammonium persulfate (APS) and, lysozyme from chicken egg white and Con A were all purchased from Sigma–Aldrich. BSA (98%) was from Amresco (Ohio, USA). PBS buffer tablets were purchased from Medicago AB. Other chemicals used were analytical grade. All reagents were used as received.

4.2. Preparation of pHEMA cryogels

Two pHEMA cryogels were produced by free radical cryocopolymerization of monomers initiated by TEMED and APS in glass columns with the inner diameters of 5 mm and 10 mm, respectively. For the preparation of cryogel in the column of 5 mm diameter (Cryogel-1), monomers (1.53 g of HEMA, 0.46 g of PEGDA and 0.27 g AGE) were dissolved in 11 ml of deionized water and the mixture was degassed with nitrogen gas for 10 min. The mixture was then cooled to 0 °C and 0.02 g of TEMED (dissolved in 1 ml of deionized water) and 0.02 g of APS (dissolved in 1 ml of deionized water) were added to the mixture to give a total volume of 15 ml and a monomer concentration of 15% (w/v). The gelation mixture was then briefly stirred and 0.8 ml was quickly added to a glass column and frozen at −12 °C for 24 h. The resulting cryogel was thawed at room temperature and washed by pumping 100 ml of deionized water through it to remove unreacted monomers. 100 ml of 0.5 M Na_2CO_3 was then pumped through the cryogel followed by 100 ml of 0.5 M IDA in 1.0 M Na_2CO_3 which was applied in a recycling mode for 18 h at room temperature. Thereafter, the cryogel was washed with 100 ml of 0.5 M Na_2CO_3 and then with water until neutral pH. The height of the obtained water swollen cryogel column was 4.8 cm. For the preparation of cryogel in the column of 10 mm diameter (Cryogel-2), the solution containing monomers with the same concentrations as those used in the preparation of Cryogel-1 was added into the glass column, which was then sealed and immersed into ethanol contained in a freezing system and frozen at −15 °C for 24 h. The obtained cryogel was thawed at room temperature and washed by deionized water for further measurements. The height of Cryogel-2 was 6.5 cm.

4.3. Measurement of breakthrough curves of proteins and characterization of cryogels

The column of Cryogel-1 was connected to an ÄKTA Explorer Chromatographic System and the extra-volume of this system was determined by measuring the time for an input tracer pulse (1%, v/v, acetone solution, UV_{280}) flowing through the system, bypassing the

column at a known flow-rate. For the breakthrough experiments, a lysozyme solution of 0.5 mg/ml in PBS buffer (pH 7.4) was employed and passed through the column under non-binding conditions, i.e., the protein molecules were non-retained or not bound in the cryogel. A sample of 3 ml was loaded for each run at a different flow velocity and the process was monitored at UV 280 nm. The column was washed by buffer between each run.

For the column of Cryogel-2, residence time distributions (RTDs) and breakthrough of proteins were measured at various flow velocities in a chromatographic system with a peristaltic pump, a switching valve and an on-line flow-through UV spectrometer, as used previously [9–11,20,21,23,32–34]. RTDs were investigated by the tracer pulse method and 150 μL of 0.5 mg/ml BSA and 0.5 mg/ml lysozyme solution were applied as the tracers in each run, respectively. The obtained response signals were then used to evaluate the axial dispersion performance within the column. The axial dispersion coefficients at different liquid flow velocities were determined by the variance and the mean residence time of the corresponding RTD curve under close-vessel boundary [10]. In the breakthrough curve measurements, the protein solution of 0.5 mg/ml of lysozyme in 20 mM PBS buffer (pH 7.4) was passed through the column at various flow velocities. The loaded sample was 15 ml for each run and the process was also monitored at UV 280 nm. The column was washed using 2 M NaCl in 20 mM PBS buffer (pH 7.4) between each run. The breakthrough curves of BSA and Con A at the same conditions were also measured.

The relationships between the pressure vs. flow rate through the cryogels were measured by passing deionized water through the columns at different hydrostatic pressure drops (i.e., using different heights of water-columns) and the cryogel permeabilities were determined by fitting the experimental data with Eq. (6). Porosities of Cryogel-1 and Cryogel-2 were determined by measuring the content of free water and the cryogel volume of a given sample as previously described in [5,6,10], and the microstructure of the cryogel was visualized and determined by scanning electron microscope (SEM), according to the procedure described by [6,7,13].

5. Results and discussion

Experimental values of the cryogel diameter, length, porosity and permeability, as well as the liquid properties, were used as the known inputs for the model. In the model calculation, viscosities and densities of the present aqueous dilute solution of lysozyme, BSA or Con A at the test concentration and temperatures were estimated using the equations reported by Monkos [85,86], as similar as in Ref. [76]. The diffusion coefficients of BSA and Con A in PBS buffer were estimated using the correlation suggested by Young et al. [87] and the diffusion coefficient of lysozyme was calculated by the equation proposed by Tyn and Gusek [88], respectively. These correlations were found to fit well with experimental data as demonstrated by He and Niemeyer [89]. Basic parameter values used in the model are summarized in Table 1.

The physical parameters of the capillaries and skeletons in the model were determined by fitting the model calculation in a manual manner with the experimental results of the cryogel size, porosity, permeability together with the protein breakthrough curves at a given flow velocity. For a typical fitting, the value of $t_{d\max}$ at a certain liquid velocity was obtained from the breakthrough curve for Cryogel-1 or the RTD curve for Cryogel-2 and the range of d_s was set as from 1 to 12 μm in this work because the skeletons of the present cryogels were very thin. Firstly, the initial values of d_m, σ, d_s and $\tau_{d\min}$ were given and the range of M was calculated by Eq. (13b). For each M, the number of capillary groups was estimated by setting the diameter step as 1 μm and the number of capillary in each group was determined by integrating Eq. (8b) between the group intervals. Then, the porosity, the permeability and the total bed volume were calculated by Eqs. (2), (3) and (7). The obtained values were compared with the corresponding experimental values and their relative errors were calculated. The allowable maximum relative error between the calculated and experimental values was set below 2% for porosity and permeability, and 1% (Cryogel-1) or 1.8% (Cryogel-2) for the total bed volume, respectively. If the obtained relative errors were larger than the allowable values, new values of these unknown parameters were generated and the calculation of the porosity, the permeability and the total bed volume was repeated again. The iterative step of $\tau_{d\min}$ was set as 0.005, which was sufficient to give a good accuracy to achieve the fitting. In order to improve the fitting efficiency and decrease the calculation time, the manual procedure for generating new values of d_m, σ and d_s was employed here, which was achieved by using iterative steps of 1, 0.1 and 0.5 μm at each new calculation, respectively. This procedure was repeated until the obtained relative errors were within the allowable values. Generally, there could be different sets of parameters in the model which can match well with the experimental values. But only those fitting well with the experimental breakthrough curve at a given flow velocity were considered as the reasonable parameters and used in the calculation. The model was solved numerically and the dispersion coefficients and breakthrough profiles of proteins under non-adsorption conditions at different flow velocities were predicted. The relative differences of the porosity, the permeability and the bed volume as well as the mean difference of the breakthrough data between the model predictions and the experimental values were calculated and listed in Table 2. These values are low, indicating satisfied predictions by the present model.

5.1. The total number and tortuosities of capillaries in the model

The total number of capillaries and the tortuosities are two crucial parameters needed to be determined by the model. From SEM images of the pHEMA cryogels shown in Fig. 2(a) and (b), the pore diameters are in the range from about 10 to 100 μm for Cryogel-1 and 10 to 110 μm for Cryogel-2. We roughly set $d_{\min} = 10$ μm for both cryogels and $d_{\max} = 100$ μm for Cryogel-1 and $d_{\max} = 110$ μm for Cryogel-2 in the calculation. For Cryogel-1, $t_{d\max}$ of 25.4 s was observed from the experimental breakthrough of lysozyme under non-adsorption conditions at the liquid flow velocity of 8.49×10^{-4} m/s, and this value was employed to determine $t_{d\max}$. For Cryogel-2, $t_{d\max}$ of 245 s was obtained from the RTD curve at the liquid flow velocity of 1.65×10^{-4} m/s. The tortuosities of different capillaries were determined using Eq. (11b) together by considering Eq. (13b), and the total number of capillaries is likely to be within the range of $2289 \le M \le 50{,}491$ for Cryogel-1 or $7763 \le M \le 261{,}284$ for Cryogel-2. A satisfactory number of 2306 capillaries for Cryogel-1 or 7791 for Cryogel-2 was obtained by fitting the model prediction with the experimental data, and this value was then employed in the following calculation. The obtained tortuosities of capillaries increased from 2.36 to 4.08 with the increase of capillary diameter from 10 to 100 μm for Cryogel-1, while from 2.10 to 6.49 with the increase of capillary diameter from 10 to 110 μm for Cryogel-2, as shown in Fig. 3.

5.2. Diameter distribution and skeleton thickness of capillaries in the model

Pore sizes and wall thickness distribution in cryogels can be assessed by imaging processing method using software like NIH ImageJ, as demonstrated recently by Dainiak et al. [90]. However, the uncertain results of image analysis may be influenced by both the image quality and the method of image processing, especially

Table 1
Basic parameters used in the model.

Column	Protein	d_c (m)	L (m)	φ (–)	k (m^2)	μ_L (Pa s)	ρ_L (kg/m^3)	D_{AB} (m^2/s)
Cryogel-1	Lysozyme	5×10^{-3}	4.8×10^{-2}	0.847	8.45×10^{-12}	1.0×10^{-3}	1002	1.18×10^{-10}
Cryogel-2	Lysozyme	10×10^{-3}	6.5×10^{-2}	0.886	5.58×10^{-12}	8.0×10^{-4}	1000	1.43×10^{-10}
Cryogel-2	BSA	10×10^{-3}	6.5×10^{-2}	0.886	5.58×10^{-12}	7.8×10^{-4}	1000	7.98×10^{-11}
Cryogel-2	Con A	10×10^{-3}	6.5×10^{-2}	0.886	5.58×10^{-12}	8.4×10^{-4}	1000	6.38×10^{-11}

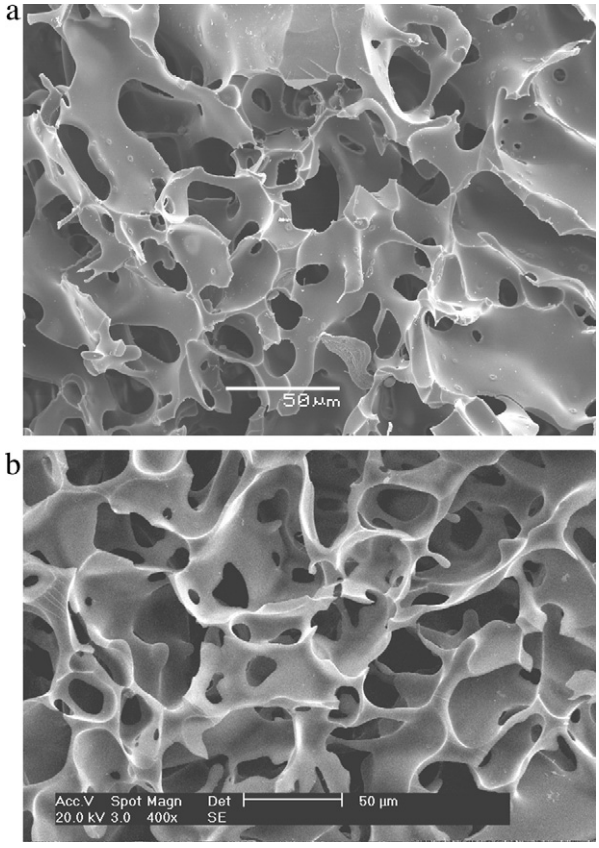

Fig. 2. Scanning electron microscope photographs of the poly(hydroxyethyl methacrylate) cryogels. (a) Cryogel-1 and (b) Cryogel-2.

the choice of threshold magnitude for the segmentation of pores and skeletons and even the pore structure heterogeneity. In the present work, we determine the unknown physical parameters of the capillaries d_s, d_m and σ by simultaneously fitting the model calculation with the experimental data of permeability, porosity, bed volume as well as the protein breakthrough curve at a given velocity. For Cryogel-1 a good agreement between the calculated and experimental data was observed for $d_m = 51$ μm, $\sigma = 13.0$ μm and $d_s = 4.5$ μm, while for Cryogel-2 the obtained values were $d_m = 46$ μm, $\sigma = 19.7$ μm and $d_s = 3.5$ μm. It should be noted that the skeleton thickness is comparable to those for pDMAA (*N*,*N*-dimethylacrylamide) cryogels reported by Persson et al. [22] and gelatin–fibrinogen cryogels by Dainiak et al. [90]. It is also seen that Cryogel-2 has a wider pore size distribution that that for Cryogel-1. The reason is that the small column diameter (5 mm diameter) gave more uniform microstructures or pores than the larger column (10 mm diameter) for the monomer solution with the same concentration under the similar freezing conditions. Based on these parameters, the calculated porosities by the model were 0.849 for Cryogel-1 and 0.882 for Cryogel-2, while the permeabilities by the model were 8.43×10^{-12} m^2 and 5.48×10^{-12} m^2, respectively. These values are very close to the experimental values listed in Table 1.

Fig. 4 shows the capillary diameter distributions in the cryogel beds given by the model. As can be seen, for Cryogel-1 the effective capillary diameters are in the range from 11 to 92 μm (correspondingly the actual tortuoses of these capillaries increased linearly from 2.37 to 3.92) and for Cryogel-2 the effective capillary diameters are in the range from 10 to 110 μm. For Cryogel-1 the contribution of capillaries with $d_i < 11$ μm and $d_i > 92$ μm was neglected. Therefore, it is expected that the actual pores could be in the range of diameters from 11 to 92 μm with the mean diameter of 51 μm in Cryogel-1 and 10 to 110 μm with the mean diameter of 46 μm in Cryogel-2, both with the normal size distribution.

In this model, we assumed a constant skeleton thickness for each cryogel. In reality, it is difficult to determine the accurate value of this parameter even from the SEM images, because the skeleton observed by SEM is not uniform (varied from about 1 to 12 μm, as shown in Fig. 2) and may be either deformed by the sample preparation process or enlarged by a change in observational position or direction. The present value of $d_s = 4.5$ μm for Cryogel-1 or $d_s = 3.5$ μm for Cryogel-2 can thus be considered as an approximate but satisfactory description of the actual skeleton thickness due to

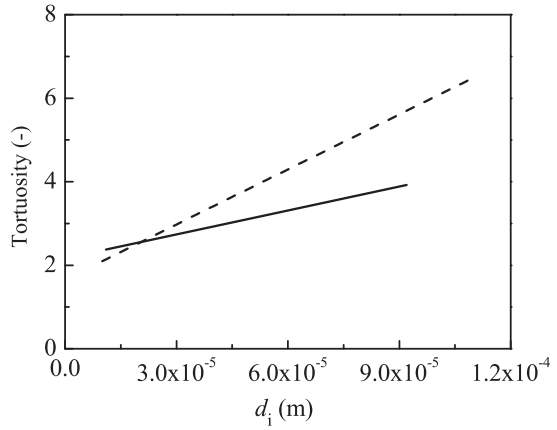

Fig. 3. Tortuosities of capillaries in the poly(hydroxyethyl methacrylate) cryogel beds in the model. (–) Cryogel-1 and (- - -) Cryogel-2.

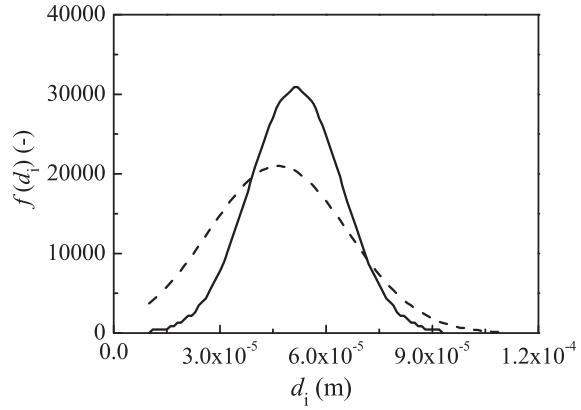

Fig. 4. Diameter distribution of capillaries in the model. (–) Cryogel-1 and (- - -) Cryogel-2.

Table 2
Deviations of the model predictions from the experimental data at various flow velocities.

Column	Protein	δ_φ	δ_k	δ_V	δ_C at different flow velocities											
					8.25 $\times 10^{-5}$ m/s	8.49 $\times 10^{-5}$ m/s	1.65 $\times 10^{-4}$ m/s	1.70 $\times 10^{-4}$ m/s	2.48 $\times 10^{-4}$ m/s	2.55 $\times 10^{-4}$ m/s	3.48 $\times 10^{-4}$ m/s	5.10 $\times 10^{-4}$ m/s	8.41 $\times 10^{-4}$ m/s	8.49 $\times 10^{-4}$ m/s	1.70 $\times 10^{-3}$ m/s	2.55 $\times 10^{-3}$ m/s
Cryogel-1	Lysozyme	0.002	0.002	0.007	–	0.043	–	0.028	–	0.028	–	–	–	0.019	0.020	0.028
Cryogel-2	Lysozyme	0.005	0.018	0.008	0.024	–	0.015	–	0.011	–	0.019	0.020	0.042	–	–	–
Cryogel-2	BSA	0.005	0.018	0.008	0.016	–	0.015	–	0.008	–	0.006	0.020	0.014	–	–	–
Cryogel-2	Con A	0.005	0.018	0.008	0.017	–	0.016	–	0.013	–	0.014	0.013	0.016	–	–	–

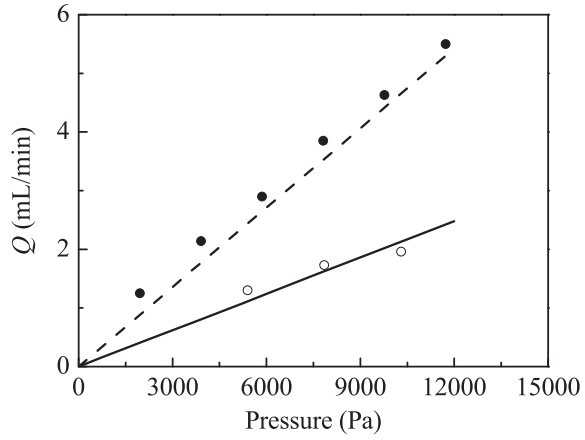

Fig. 5. Comparison of the experimental values of flow rate vs. pressure drop with the data calculated by the model in the poly(hydroxyethyl methacrylate) cryogel beds. (○) experimental in Cryogel-1, (●) experimental in Cryogel-2, (–) predicted in Cryogel-1, and (- - -) predicted in Cryogel-2.

the good agreement between the calculated and experimental data of porosity, permeability and bed volume. These parameters represent suitable values and the presented model itself could thus be regarded as successful in giving a good description of the actual pHEMA cryogel bed.

5.3. Flow rate vs. pressure and axial dispersion

The permeabilities of the cryogels obtained by fitting the experimental data of flow rate vs. pressure drop with Darcy's equation are 8.45×10^{-12} m^2 for Cryogel-1 (the correlation coefficient $R = 0.984$) and 5.58×10^{-12} m^2 for Cryogel-2 ($R = 0.986$), respectively. Fig. 5 displays the comparisons between the experimental values and the calculated data of flow rate vs. pressure drop by the model in the cryogel beds. As can be seen, the agreement between the calculated data by the model and the experimental values is good within the range of flow rates considered.

The axial dispersion coefficients of lysozyme within different capillaries in Cryogel-1 were calculated by Eqs. (10a) and (10b) in the model and shown in Fig. 6. As can be seen, the values of D_{axi} increase both with the increase of capillary diameter and flow velocity. These values are for most capillaries much higher than the molecular diffusion coefficient of lysozyme. Similar results were observed in Cryogel-2 (data not shown here).

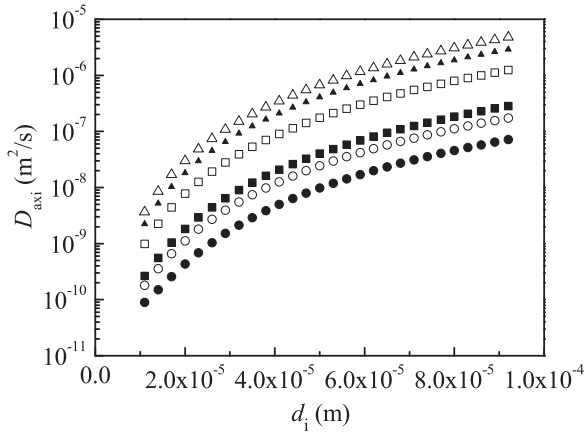

Fig. 6. Variation of axial dispersion coefficients with capillary diameter in Cryogel-1 at liquid flow velocities of 8.49×10^{-5} (●), 1.70×10^{-4} (○), 2.55×10^{-4} (■), 8.49×10^{-4} (□), 1.70×10^{-3} (▲) and 2.55×10^{-3} (Δ) m/s, respectively.

In reality, it is very difficult to obtain the experimental data of axial dispersion coefficients in each supermacropore within an actual cryogel bed and thus, we cannot compare the calculated dispersion directly with experimental data in each capillary. Alternatively, the mean axial dispersion coefficient in all these capillaries according to their flow rates was considered as the calculated dispersion coefficient by the model, which can be determined by the equation expressed as

$$D_{ax} = \frac{\sum_{i}^{N_g} D_{axi} n_i Q_i}{Q} \quad (16)$$

The axial dispersion coefficients in Cryogel-2 at the flow velocities of 8.25×10^{-5}, 1.65×10^{-4}, 2.48×10^{-4}, 3.48×10^{-4}, 5.10×10^{-4}, and 8.41×10^{-4} m/s were determined by RTDs using BSA and lysozyme as tracers, respectively. The obtained results are shown in Fig. 7. It is seen that the dispersion coefficients increased from 6.59×10^{-8} to 5.00×10^{-7} m^2/s for lysozyme and 4.66×10^{-8} to 5.12×10^{-7} m^2/s for BSA with the increase of flow velocity from 8.25×10^{-5} to 8.41×10^{-4} m/s. The mean axial dispersion coefficients were also calculated by the model at the same flow velocities and the obtained values were compared with the experimental, as also shown in Fig. 7. It can be seen that the agreement between the calculated and experimental data is good, indicating that Eq. (10b) is valid in the estimation of axial dispersion coefficients and could be employed in describing the axial dispersion within capillaries in these cryogel beds.

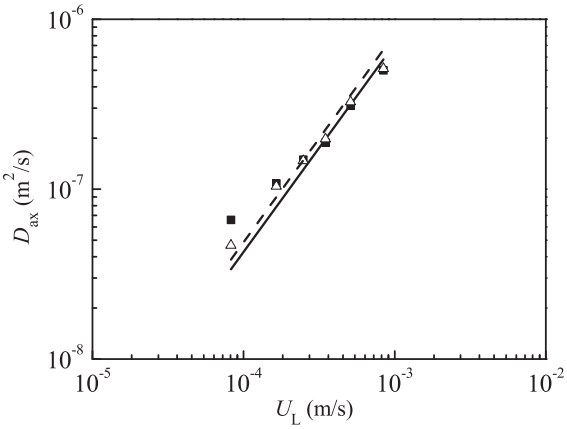

Fig. 7. Comparison of the predicted and experimental mean axial dispersion coefficients at various liquid velocities in Cryogel-2. (■) lysozyme, experimental, (Δ) bovine serum albumin, experimental, (–) lysozyme, predicted and (- - -) bovine serum albumin, predicted.

5.4. Breakthrough curves of proteins under non-adsorption condition

In this work, three different proteins, i.e., lysozyme, BSA and Con A, were employed as the model proteins to test the model under non-adsorption conditions. Molecular weights of these proteins are 14.3, 67 and 102 kDa, respectively. For Cryogel-1, breakthrough curves of lysozyme at the liquid velocities of 8.49×10^{-5}, 1.70×10^{-4}, 2.55×10^{-4}, 8.49×10^{-4}, 1.70×10^{-3} and 2.55×10^{-3} m/s were obtained. It was observed that in these runs the binding capacity of protein molecules due to the possible IDA functional groups was very low (below 0.006 mg/ml cryogel)

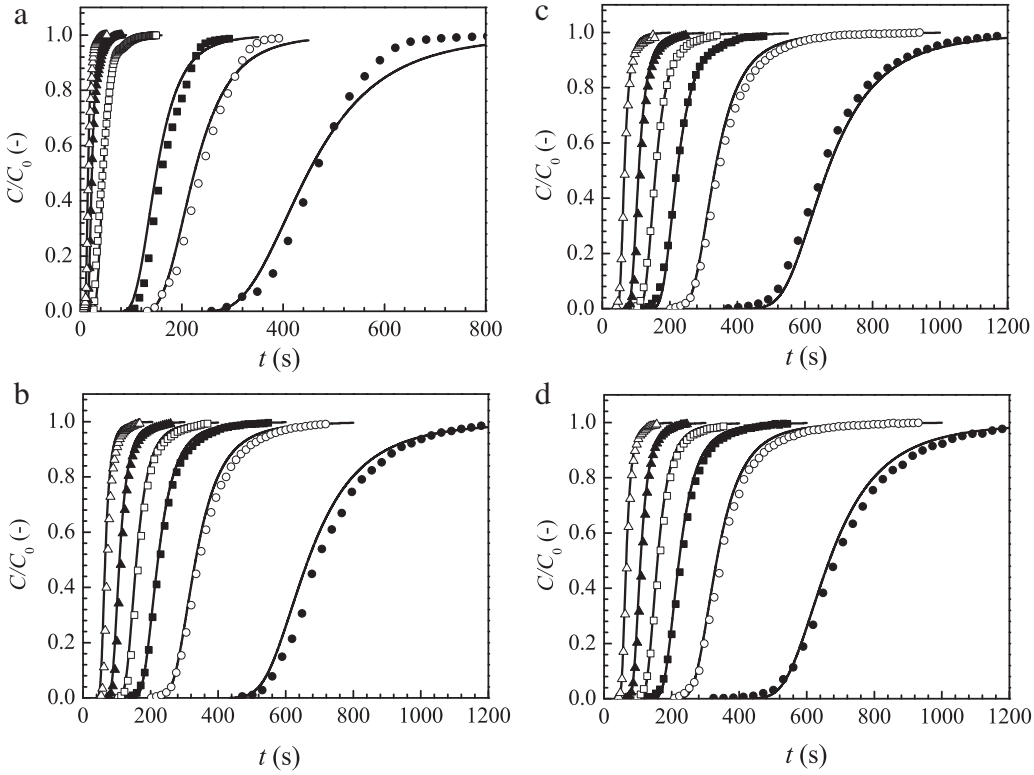

Fig. 8. Comparison of the predicted and experimental breakthrough curves of proteins under non-adsorption condition at various liquid velocities. (a) Lysozyme in Cryogel-1, (b) lysozyme in Cryogel-2, (c) bovine serum albumin in Cryogel-2 and (d) concanavalin A in Cryogel-2. The liquid velocities in Cryogel-1 are 8.49×10^{-5} (●), 1.70×10^{-4} (○), 2.55×10^{-4} (■), 8.49×10^{-4} (□), 1.70×10^{-3} (▲) and 2.55×10^{-3} (Δ) m/s, respectively. The liquid velocities in Cryogel-2 are 8.25×10^{-5} (●), 1.65×10^{-4} (○), 2.48×10^{-4} (■), 3.48×10^{-4} (□), 5.10×10^{-4} (▲) and 8.41×10^{-4} (Δ) m/s, respectively. The solid lines represent the calculation results by the model.

and thus was neglected. For Cryogel-2, breakthrough curves of lysozyme, BSA and Con A are measured at the liquid velocities of 8.25×10^{-5}, 1.65×10^{-4}, 2.48×10^{-4}, 3.48×10^{-4}, 5.10×10^{-4}, and 8.41×10^{-4} m/s, respectively. No binding of proteins was observed. Therefore, in both cryogels the non-binding assumption was valid and protein molecules passed through the pores of the cryogels freely without being bound. Under non-adsorption conditions, the mass balance equation was solved by the finite difference method and the breakthrough profiles were calculated by the model at the corresponding flow velocities as the experiments. In the solving process, each capillary was divided into 50 cells and time steps of 0.1 s were used in the calculation. There was no obvious improvement of accuracy connected with further decreasing the time step or distance interval step.

Fig. 8 shows the comparisons of the calculated results of breakthrough of the considered proteins with the experimental data (expressed as the symbols) at various velocities in Cryogel-1 and Cryogel-2. As it is seen the model predictions are in good agreement with the experimental data, though when varying the values of the different parameters, other likely fittings with the experimental data could be obtained. Therefore, further optimizations based on the precise experimental determination of the parameters are worthy of being investigated in future as it seems that the accuracy of these parameters is very important for the model prediction.

6. Conclusions

The presented model has been shown to be effective in characterizing the microstructure of a cryogel bed and in describing the liquid flow and mass transfer behaviors within supermacropores. The pore tortuosity and the skeleton thickness are considered in this model, and this gives a more detailed model description of an actual cryogel. The parameters of capillaries in the model can be determined by fitting experimental data of permeability, porosity, cryogel bed volume and breakthrough curve under the non-adsorption condition. Once these parameters are determined, the model can then be used to predict the behaviors of protein breakthrough profiles at different flow velocities. Based on the model predictions we have found that the effective pore sizes of the considered pHEMA cryogels are likely be in the range of 10–90 μm for Cryogel-1 and 10–110 μm for Cryogel-2. The mean pore diameters for these two cryogels are likely to be around 51 and 46 μm, and both these calculated predictions show to be close to the actual values of the pores observed from the SEM image. The next step in the development of a comprehensive model of chromatographic performance of cryogels would be the study of breakthrough profiles under the binding conditions. This was the motivation behind the synthesis and study both the plain and IDA-containing pHEMA cryogels, which are the basic matrix for further preparation of ion exchange, hydrophobic and immobilized metal ion affinity cryogels, albeit the IDA-functionality has not been exploited further in the present work.

Acknowledgements

This work was supported by Swedish Research Council. Junxian Yun acknowleges the financial support by the State Scholarship from the China Scholarship Council, the Science and Technology Cooperation Project between China-Europe Country's Governments from the Ministry of Science and Technology of China (Grant No. 1017), the National Natural Science Foundation of China (Nos. 20876145, 21036005) and the Zhejiang Provincial Natural Science Foundation of China (No. Y4080326). The authors also thank Dongjiao Zhou for cryogel measurements.

References

[1] V.I. Lozinsky, F.M. Plieva, I.Y. Galaev, B. Mattiasson, Bioseparation 10 (2002) 163.
[2] V.I. Lozinsky, I.Y. Galaev, F.M. Plieva, I.N. Savina, H. Jungvid, B. Mattiasson, Trends Biotechnol. 21 (2003) 445.
[3] F.M. Plieva, I.Y. Galaev, B. Mattiasson, J. Sep. Sci. 30 (2007) 1657.
[4] V.I. Lozinsky, Russ. Chem. Rev. 71 (2002) 489.
[5] P. Arvidsson, F.M. Plieva, V.I. Lozinsky, I.Y. Galaev, B. Mattiasson, J. Chromatogr. A 986 (2003) 275.
[6] F.M. Plieva, I.N. Savina, S. Deraz, J. Andersson, I.Y. Galaev, B. Mattiasson, J. Chromatogr. B 807 (2004) 129.
[7] F.M. Plieva, J. Andersson, I.Y. Galaev, B. Mattiasson, J. Sep. Sci. 27 (2004) 828.
[8] F.M. Plieva, M. Karlsson, M.R. Aguilar, D. Gomez, S. Mikhalovsky, I.Y. Galaev, B. Mattiasson, J. Appl. Polym. Sci. 100 (2006) 1057.
[9] K.J. Yao, S.C. Shen, J.X. Yun, L.H. Wang, X.J. He, X.M. Yu, Chem. Eng. Sci. 61 (2006) 6701.
[10] K.J. Yao, J.X. Yun, S.C. Shen, L.H. Wang, X.J. He, X.M. Yu, J. Chromatogr. A 1109 (2006) 103.
[11] X.J. He, K.J. Yao, S.C. Shen, J.X. Yun, Chem. Eng. Sci. 62 (2007) 1334.
[12] R.V. Ivanov, V.I. Lozinsky, S.K. Noh, S.S. Han, W.S. Lyoo, J. Appl. Polym. Sci. 106 (2007) 1470.
[13] H. Kirsebom, G. Rata, D. Topgaard, B. Mattiasson, I.Y. Galaev, Polymer 49 (2008) 3855.
[14] G. Baydemir, N. Bereli, M. Andaç, R. Say, I.Y. Galaev, A. Denizli, Funct. Polym. 69 (2009) 36.
[15] I.N. Savina, I.Y. Galaev, B. Mattiasson, J. Chromatogr. A 1092 (2005) 199.
[16] I.N. Savina, B. Mattiasson, I.Y. Galaev, Polymer 46 (2005) 9596.
[17] I.N. Savina, I.Y. Galaev, B. Mattiasson, J. Mol. Recogn. 19 (2006) 313.
[18] I.N. Savina, B. Mattiasson, I.Y. Galaev, J. Polym. Sci. Part A: Polym. Chem. 44 (2006) 1952.
[19] F.M. Plieva, B. Bober, M. Dainiak, I.Y. Galaev, B. Mattiasson, J. Mol. Recogn. 19 (2006) 305.
[20] K.J. Yao, J.X. Yun, S.C. Shen, F. Chen, J. Chromatogr. A 1157 (2007) 246.
[21] F. Chen, K.J. Yao, J.X. Yun, S.C. Shen, Chem. Eng. Sci. 63 (2008) 71.
[22] P. Persson, O. Baybak, F.M. Plieva, I.Y. Galaev, B. Mattiasson, B. Nilsson, A. Axelsson, Biotechnol. Bioeng. 88 (2004) 224.
[23] K.J. Yao, S.C. Shen, J.X. Yun, L.H. Wang, F. Chen, X.M. Yu, Biochem. Eng. J. 36 (2007) 139.
[24] F. Yılmaz, N. Bereli, H. Yavuz, A. Denizli, Biochem. Eng. J. 43 (2009) 272.
[25] F.M. Plieva, E.D. Seta, I.Y. Galaev, B. Mattiasson, Sep. Purif. Technol. 65 (2009) 110.
[26] P. Arvidsson, F.M. Plieva, I.N. Savina, V.I. Lozinsky, S. Fexby, L. Bulow, I.Y. Galaev, B. Mattiasson, J. Chromatogr. A 977 (2002) 27.
[27] M.B. Dainiak, A. Kumara, F.M. Plieva, I.Y. Galaev, B. Mattiasson, J. Chromatogr. A 1045 (2004) 93.
[28] A. Hanora, F.M. Plieva, M. Hedström, I.Y. Galaev, B. Mattiasson, J. Biotechnol. 118 (2005) 421.
[29] A. Kumar, V. Bansal, K.S. Nandakumar, I.Y. Galaev, P.K. Roychoudhury, R. Holmdah, B. Mattiasson, Biotechnol. Bioeng. 93 (2006) 636.
[30] A. Hanora, I.N. Savina, F.M. Plieva, V.A. Izumrudov, B. Mattiasson, I.Y. Galaev, J. Biotechnol. 123 (2006) 343.
[31] S. Deraz, F.M. Plieva, I.Y. Galaev, E.N. Karlsson, B. Mattiasson, Enzyme Microb. Technol. 40 (2007) 786.
[32] J.X. Yun, S.C. Shen, F. Chen, K.J. Yao, J. Chromatogr. B 860 (2007) 57.
[33] L.H. Wang, S.C. Shen, J.X. Yun, K.J. Yao, S.J. Yao, J. Sep. Sci. 31 (2008) 689.
[34] Y. Chen, S.C. Shen, J.X. Yun, K.J. Yao, J. Sep. Sci. 31 (2008) 3879.
[35] F.M. Plieva, I.Y. Galaev, W. Noppe, B. Mattiasson, Trends Microbiol. 16 (2008) 543.
[36] J.J. Meyers, A.I. Liapis, J. Chromatogr. A 827 (1998) 197.
[37] J.J. Meyers, A.I. Liapis, J. Chromatogr. A 852 (1999) 3.
[38] A.I. Liapis, J.J. Meyers, O.K. Crosser, J. Chromatogr. A 865 (1999) 13.
[39] K. Kaczmarski, D. Antos, H. Sajonz, P. Sajonz, G. Guiochon, J. Chromatogr. A 925 (2001) 1.
[40] A.R. Özdural, A. Alkan, P.J.A.M. Kerkhof, J. Chromatogr. A 1041 (2004) 77.
[41] W. Li, Y. Li, Y. Sun, Chem. Eng. Sci. 60 (2005) 4780.
[42] M. Zabka, M. Minceva, A.E. Rodrigues, Chem. Eng. Process. 45 (2006) 150.
[43] M.A. Hashim, K.H. Chu, Sep. Purif. Technol. 53 (2007) 189.
[44] M. Zabka, M. Minceva, A.E. Rodrigues, J. Biochem. Biophys. Methods 70 (2007) 95.
[45] R. Gutsche, G. Bunke, Chem. Eng. Sci. 63 (2008) 4203.
[46] L. Melter, A. Butté, M. Morbidelli, J. Chromatogr. A 1200 (2008) 156.
[47] N. Forrer, A. Butté, M. Morbidelli, J. Chromatogr. A 1214 (2008) 71.
[48] F. Augier, C. Laroche, E. Brehon, Sep. Purif. Technol. 63 (2008) 466.
[49] G. Guiochon, A. Felinger, D.G. Shirazi, A.M. Katti, Fundamentals of Preparative and Nonlinear Chromatography, 2nd ed., Elsevier, Amsterdam, The Netherlands, 2006.
[50] J.C. Giddings, Dynamics of Chromatography, Part I, Principles and Theory, Marcel Dekker, New York, 1965.
[51] F. Gritti, W. Piatkowski, G. Guiochon, J. Chromatogr. A 978 (2002) 81.
[52] F. Gritti, W. Piatkowski, G. Guiochon, J. Chromatogr. A 983 (2003) 51.
[53] H. Minakuchi, K. Nakanishi, N. Soga, N. Ishizuka, N. Tanaka, J. Chromatogr. A 762 (1997) 135.
[54] H. Minakuchi, K. Nakanischi, N. Soga, N. Ishizuka, N. Tanaka, J. Chromatogr. A 797 (1998) 121.
[55] R. Hahn, A. Jungbauer, Anal. Chem. 72 (2000) 4853.

[56] F.C. Leinweber, D. Lubda, K. Cabrera, U. Tallarek, Anal. Chem. 74 (2002) 2470.
[57] U. Tallarek, F.C. Leinweber, A. Seidel-Morgenstern, Chem. Eng. Technol. 25 (2002) 12.
[58] R. Skudas, B.A. Grimes, M. Thommes, K.K. Unger, J. Chromatogr. A 1216 (2009) 2625.
[59] K. Miyabe, G. Guiochon, J. Phys. Chem. B 106 (2002) 8898.
[60] K. Miyabe, A. Cavazzini, F. Gritti, M. Kele, G. Guiochon, Anal. Chem. 75 (2003) 6975.
[61] K. Miyabe, G. Guiochon, J. Sep. Sci. 27 (2004) 853.
[62] F. Gritti, R. Skudas, K.K. Unger, D. Lubda, J. Chromatogr. A 1144 (2007) 14.
[63] N. Vervoort, P. Gzil, G.V. Baron, G. Desmet, Anal. Chem. 75 (2003) 843.
[64] N. Vervoort, H. Saito, K. Nakanishi, G. Desmet, Anal. Chem. 77 (2005) 3986.
[65] P. Gzil, N. Vervoort, G.V. Baron, G. Desmet, J. Sep. Sci. 27 (2004) 887.
[66] P. Gzil, J.D. Smet, G. Desmet, J. Sep. Sci. 29 (2006) 1675.
[67] F. Detobel, P. Gzil, G. Desmet, J. Sep. Sci. 32 (2009) 2707.
[68] D. Hlushkou, S. Bruns, U. Tallarek, J. Chromatogr. A 1217 (2010) 3674.
[69] D. Hlushkou, S. Bruns, A. Höltzel, U. Tallarek, Anal. Chem. 82 (2010) 7150.
[70] E.I. Trilisky, H. Kokua, K.J. Czymmek, A.M. Lenhoff, J. Chromatogr. A 1216 (2009) 6365.
[71] G. Guiochon, J. Chromatogr. A 1168 (2007) 101.
[72] K.K. Unger, R. Skudas, M.M. Schulte, J. Chromatogr. A 1184 (2008) 393.
[73] A. Jungbauer, R. Hahn, J. Chromatogr. A 1184 (2008) 62.
[74] J.C. Giddings, Unified Separation Science, Wiley, New York, 1991.
[75] J.X. Yun, H. Kirsebom, I.Y. Galaev, B. Mattiasson, J. Sep. Sci. 32 (2009) 2601.
[76] J.X. Yun, D.Q. Lin, S.J. Yao, J. Chromatogr. A 1095 (2005) 16.
[77] R. Aris, Proc. R. Soc. A 235 (1956) 67.
[78] O. Levenspiel, Ind. Eng. Chem. 50 (1958) 343.
[79] K.B. Bischoff, O. Levenspiel, Chem. Eng. Sci. 17 (1962) 245.
[80] J. Dayan, O. Levenspiel, Ind. Eng. Chem. Fund. 8 (1969) 840.
[81] O. Levenspiel, Chemical Reaction Engineering, 3rd ed., Wiley, New York, 1999.
[82] G. Taylor, Proc. R. Soc. A 219 (1953) 186.
[83] R.J. Nunge, T.-S. Lin, W.N. Gill, J. Fluid Mech. 51 (1972) 363.
[84] C.B. Minnich, F. Sipeer, L. Greiner, M.A. Liauw, Ind. Eng. Chem. Res. 49 (2010) 5530.
[85] K. Monkos, Int. J. Biol. Macromol. 18 (1996) 61.
[86] K. Monkos, Biochim. Biophys. Acta 1339 (1997) 304.
[87] M.E. Young, P.A. Carroad, R.L. Bell, Biotechnol. Bioeng. 22 (1980) 947.
[88] M.T. Tyn, T.W. Gusek, Biotechnol. Bioeng. 35 (1990) 327.
[89] L.Z. He, B. Niemeyer, Biotechnol. Prog. 19 (2003) 544.
[90] M.B. Dainiak, I.U. Allan, I.N. Savina, L. Cornelio, E.S. James, S.L. James, S.V. Mikhalovsky, H. Jungvid, I.Y. Galaev, Biomaterials 31 (2010) 67.